Calcium-Dependent Structural Coupling between Opposing Globular Domains of Calmodulin Involves the Central Helix†

Hongye Sun, Dan Yin, and Thomas C. Squier*

Biochemistry and Biophysics Section, Department of Molecular Biosciences, University of Kansas, Lawrence, Kansas 66045-2106

Received August 4, 1998; Revised Manuscript Received July 9, 1999

ABSTRACT: We have used fluorescence spectroscopy to investigate the average structure and extent of conformational heterogeneity associated with the central helix in calmodulin (CaM), a sequence that contributes to calcium binding sites 2 and 3 and connects the amino- and carboxyl-terminal globular domains. Using site-directed mutagenesis, a double mutant was constructed involving conservative substitution of $Tyr^{99} \rightarrow Trp^{99}$ and $Leu^{69} \rightarrow Cys^{69}$ with no significant effect on the secondary structure of CaM. These mutation sites are at opposite ends of the central helix. Trp^{99} acts as a fluorescence resonance energy transfer (FRET) donor in distance measurements of the conformation of the central helix. Cys^{69} provides a reactive group for the covalent attachment of the FRET acceptor 5-((((2-iodoacetyl)amino)-ethyl)amino)naphthalene-1-sulfonic acid (IAEDANS). AEDANS-modified CaM fully activates the plasma membrane (PM) Ca-ATPase, indicating that the native structure is retained following site-directed mutagenesis and chemical modification. We find that the average spatial separation between Trp^{99} and AEDANS covalently bound to Cys^{69} decreases by approximately 7 ± 2 Å upon calcium binding. However, irrespective of calcium binding, there is little change in the conformational heterogeneity associated with the central helix under physiologically relevant conditions (i.e., pH 7.5, 0.1 M KCl). These results indicate that calcium activation alters the spatial arrangement of the opposing globular domains between two defined conformations. In contrast, under conditions of low ionic strength or pH the structure of CaM is altered and the conformational heterogeneity of the central helix is decreased upon calcium activation. These results suggest the presence of important ionizable groups that affect the structure of the central helix, which may play an important role in mediating the ability of CaM to rapidly bind and activate target proteins.

Calmodulin (CaM)[1] functions to amplify intracellular calcium signals in all eukaryotic cells, and mediates a wide range of cellular responses important to muscle contraction, synaptic plasticity, energy metabolism, and the maintenance of cellular homeostasis (*1*). Upon calcium binding to the high-affinity sites, located on both amino- and carboxyl-terminal domains, there is a reorientation of α-helical elements within each globular domain (*2*−*5*). These structural changes result in a more open conformation that exposes hydrophobic surfaces and specific ionic groups important to the association of both globular domains in CaM and a wide range of different target proteins (*6*, *7*). While there is general agreement concerning the tertiary structures of each of the opposing globular domains, the solution structure of the central helix remains controversial (*8*). Therefore, while the crystal structure of calcium-saturated CaM indicates that CaM contains two homologous globular domains which include an extended eight-turn α-helix often referred to as the central helix (*9*−*11*), high-field NMR measurements suggest that in solution the central helix is disrupted between Asp^{78} and Ser^{81}, resulting in the *independent* rotational motion of the opposing globular domains of CaM (*7*, *12*−*13*). However, the observed structural uncoupling between the opposing globular domains observed using NMR spectroscopy is inconsistent with a range of other biochemical and biophysical measurements, including small-angle X-ray scattering and time-resolved fluorescence spectroscopy, which suggest that there are important structural transitions associated with each of the opposing globular domains upon calcium activation that result in concerted conformational changes involving both amino- and carboxyl-terminal domains (*6*, *14*−*33*).

† Supported by National Institutes of Health Grant AG 12993 and an instrumentation grant from the National Science Foundation (BIR-9116212).

* Correspondence should be addressed to this author. Tel: (785)-864-4008. Fax: (785)-864-5321. E-mail: TCSQUIER@EAGLE.CC.UKANS.EDU.

[1] Abbreviations: CaM, calmodulin; DTNB, 5,5′-dithiobis(2-nitrobenzoic acid); EGTA, ethylene glycol bis(β-aminoethyl ether)-*N*,*N*,*N*′,*N*′-tetraacetic acid; ESI-MS, electrospray ionization mass spectrometry; FRET, fluorescence resonance energy transfer; HEPES, *N*-(2-hydroxyethyl)piperazine-*N*′-2-ethansulfonic acid; HPLC, high-performance liquid chromatography; HW, full width at half-height of a Gaussian distance distribution; IAEDANS, 5-((((2-iodoacetyl)amino)ethyl) amino)naphthalene-1-sulfonic acid; NATA, *N*-acetyl-L-tryptophanamide; *P*, steady-state polarization; r_{app}, apparent distance between donor and acceptor chromophores; r_0, initial anisotropy at time 0, R_{av}, average distance between donor and acceptor chromophores; SDS−PAGE, sodium dodecyl sulfate−polyacrylamide gel electrophoresis; $\langle\tau\rangle$, average fluorescence lifetime; $\bar{\tau}$, mean fluorescence lifetime; ϕ, rotational correlation time.

10.1021/bi9818671 CCC: $18.00
Published on Web 09/03/1999

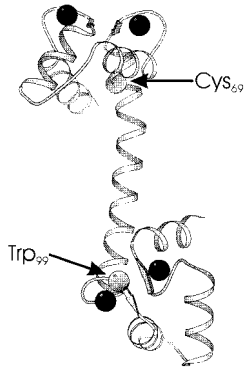

FIGURE 1: Positions of donor and acceptor chromophores within calmodulin. Relative positions of Trp^{99} and Cys^{69} (light gray spheres) are highlighted relative to the four high-affinity calcium binding sites (black spheres). Ribbons represent the protein backbone of CaM, while arrows represent antiparallel β-sheet elements. Coordinates are taken from the Brookhaven Protein Data Bank file 1cll.pdb (*11*). This illustration was created using MolScript (*93*).

The apparent discrepancy between results obtained using NMR spectroscopy and these later results may be related to the fact that NMR spectroscopy detects only conformational states that are both highly populated and long-lived (*34*). Thus, the mechanisms associated with the structural linkage between the opposing globular domains may involve (i) transient interactions between the amino- and carboxyl-terminal globular domains that result in only a small fraction of short-lived intermediates or (ii) concerted structural interactions mediated through a conformationally disordered central helix that undergoes structural rearrangements on a time scale that is slow compared with that of rotational diffusion. Alternatively, observed differences in the average structure of the long central helix using X-ray crystallography and NMR spectroscopy may be functionally important and could result from differences in experimental conditions (*35, 36*). In this regard, the predicted instability of the central helix may be functionally important (*37*−*40*), since the sequence between amino acids Arg^{74} and Glu^{82} becomes structurally disordered upon CaM binding to peptides that are identical to the CaM binding sequences of target proteins (*41*−*43*). Therefore, the conformation of the central helix may define the relative orientation of the opposing globular domains that ensures the rapid and productive interaction between CaM and a range of different target proteins (*6*). Thus, the relationship between the structure of the central helix and the ability of CaM rapidly to associate with and activate a range of different target proteins remains a central question with respect to understanding calcium signaling in eukaryotic cells.

To further investigate the solution structure of the central helix in CaM, we have used fluorescence resonance energy transfer (FRET) to measure the average spatial separation and conformational heterogeneity between chromophoric groups proximal to the opposing ends of the central helix (Figure 1). Complementary measurements of the solvent accessibilities and rotational dynamics of these chromophores permit the resolution of alterations in the local environment of these chromophores or global structural changes affecting the hydrodynamic volume of CaM. These measurements involve the conservative substitution of $Leu^{69} \rightarrow Cys^{69}$ and $Tyr^{99} \rightarrow Trp^{99}$. Trp^{99} both functions as a fluorescent reporter group of structural alterations involving the carboxyl-terminal globular domain and serves as a FRET donor. Cys^{69} permits the covalent attachment of IAEDANS, which functions as a FRET acceptor. Lifetime-resolved fluorescence resonance energy transfer (FRET) measurements permit the resolution of the spatial separation and conformational heterogeneity between these engineered sites. Additional measurements of the solvent accessibility, lifetime, and rotational dynamics of either Trp^{99} or AEDANS bound to Cys^{69} provide complementary information regarding the structural alterations in the local environment around these chromophores and with respect to the overall dimensions of CaM.

EXPERIMENTAL PROCEDURES

Materials. 5-((((2-Iodoacetyl)amino)ethyl)amino)naphthalene-1-sulfonic acid (IAEDANS) was obtained from Molecular Probes, Inc. (Eugene, OR). WP PEI (weak anion exchanger) packing for the HPLC column was from J. T. Baker (Phillipsburg, NJ), and the weak anion-exchange column used to purify CaM was packed in-house. A Micro BCA protein assay reagent kit was obtained from Pierce (Rockford, IL). Porcine erythrocyte ghost membranes were prepared at 0 °C in an ice bath, essentially as previously described (*44*). All other chemicals were of the purest grade commercially available.

Expression and Purification of Calmodulin Mutants. The coding region for chicken CaM was excised from the plasmid pCaMPL provided by Professor Samuel George (Duke University) using restriction enzymes *Nco*I and *Xba*I, and subcloned into the mutagenesis and expression vector pALTER-Ex1 (Promega, Madison, WI). The recombinant plasmid pEx1-CaM was transformed into *Escherichia coli* strain JM109(DE3) for overexpression, as previously described (*45*). Site-directed mutagenesis was carried out as described in the technical manual for the Altered Sites II in vitro mutagenesis system (Promega, Madison, WI). Oligonucleotide primers containing the desired mutation were synthesized by Macromolecular Resources (Colorado State University, Ft. Collins, CO). Correct mutations were ensured by automated DNA sequencing performed in the Biochemical Research Service Laboratory (University of Kansas, Lawrence, KS). Overexpressed CaM was purified as previously described using phenyl-Sepharose CL-4B (Pharmacia, Piscataway, NJ) and weak anion-exchange HPLC (*46, 47*). The purity of the expressed proteins was greater than 99% as indicated by SDS−PAGE and electrospray ionization mass spectrometry (ESI-MS).

Specific Derivatization of Cys^{69} in Genetically Engineered CaM. Prior to chemical derivatization, CaM was incubated in 30 mM HEPES (pH 7.5), 1.0 mM EGTA, and 50 mM DTT at room temperature for 3 h to eliminate possible intermolecular cross-linking. Following the addition of 1.0 mM $CaCl_2$, CaM was bound to a phenyl-Sepharose CL-4B affinity column, and DTT was removed by exhaustively washing the column with 50 mM HEPES (pH 7.5) and 0.1 mM $CaCl_2$. The reduced calmodulin was subsequently eluted from the column in 50 mM HEPES (pH 7.5) and 1.0 mM EGTA. Chemical derivatization of Cys^{69} was carried out in the dark and involved the addition of 60 μM IAEDANS to a solution containing 6 μM calmodulin (0.1 mg/ml) in 30 mM HEPES (pH 7.5), 1 mM EGTA, and 6.0 M guanidine

hydrochloride. The reaction was stopped after 4 h by the addition of 1 mM β-mercaptoethanol. CaM was again loaded onto a phenyl-Sepharose CL-4B affinity column, the free probe and β-mercaptoethanol were removed, and the labeled CaM was eluted from the column (see above). Chemically derivatized CaM was subsequently lyophilized following exhaustive dialysis against 5 mM ammonium bicarbonate buffer (pH 8.0).

Protein Concentration Determination and Enzymatic Assay. CaM concentration was typically measured using the micro BCA assay (Rockford, IL), using desalted CaM as a protein standard (ϵ_{277nm} = 3029 M^{-1} cm^{-1}; *46*). The erythrocyte ghost membrane protein concentration was determined by the Biuret method (*48*), using BSA as the standard. Rates of ATP hydrolysis of the plasma membrane (PM) Ca-ATPase were determined by measuring phosphate release, as previously described (*49*).

Determination of Free CaM Concentrations. The concentrations of CaM free in solution were obtained from the relationship:

$$[\mathrm{CaM}]_{\mathrm{free}} = [\mathrm{CaM}]_{\mathrm{total}} - \frac{(V - V_{\mathrm{min}})}{(V_{\mathrm{max}} - V_{\mathrm{min}})}[\mathrm{PMCA}]_{\mathrm{max}} \quad (1)$$

where V_{max} is the maximal calmodulin-dependent ATPase activity, V is the observed ATPase activity at a defined concentration of CaM, $[CaM]_{free}$ is the concentration of CaM free in solution, $[CaM]_{total}$ is the total concentration of CaM added to the solution, and [PMCA] is the total binding capacity of the PM Ca-ATPase in erythrocyte ghosts for CaM, which is the only high-affinity CaM binding protein and was previously estimated to correspond to 40 pmol of CaM bound/mg of porcine erythrocyte ghost (*50*).

Determination of Binding Affinities between CaM and the PM Ca-ATPase. The CaM-dependent activation of the PM Ca-ATPase by CaM was used to determine the apparent affinity between CaM and the CaM binding sequence of PM Ca-ATPase. This analysis takes into account that CaM contains two binding domains that must both associate with binding sites within the CaM binding sequence of the PM Ca-ATPase to affect enzyme activation. Initial binding between CaM and target proteins, including the PM Ca-ATPase, involves the association of the carboxyl-terminal domain (*7, 51, 52*). Subsequent association of the amino-terminal domain is aided by the reduced volume available for diffusion of the amino-terminal domain (*51, 53*). Therefore, the concentration of the amino-terminal domain available for binding is equal to that of the carboxyl-terminal domain of CaM bound to the PM Ca-ATPase. The calmodulin-dependent activation of the PM Ca-ATPase was therefore fit to eq 2, which takes into account the sequential and ordered binding mechanism of CaM with the Ca-ATPase:

$$\text{activity} = \frac{[\mathrm{PMCA}]_{\mathrm{free}} K_2 [\mathrm{CaM}]^2_{\mathrm{free}}}{(1 + K_1[\mathrm{CaM}]_{\mathrm{free}} + K_2[\mathrm{CaM}]^2_{\mathrm{free}})} \times \text{span} + \text{minimum} \quad (2)$$

where

$$[\mathrm{PMCA}]_{\mathrm{free}} = \frac{-1 + (1 + 4K_2[\mathrm{CaM}]^2_{\mathrm{free}}[\mathrm{PMCA}]_{\mathrm{total}})^{1/2}}{2K_2[\mathrm{CaM}]^2_{\mathrm{free}}} \quad (3)$$

Span is the CaM-dependent enzymatic activity, minimum represents the CaM-independent enzymatic activity, and activity represents the enzyme activation resulting from the association of both CaM domains with the Ca-ATPase. $[CaM]_{free}$ is the concentration of CaM not bound to the PM Ca-ATPase. $[PMCA]_{total}$ and $[PMCA]_{free}$, respectively, represent the total concentration of the Ca-ATPase and the concentration of the Ca-ATPase with no CaM bound. K_1 corresponds to the association constant k_1 associated with binding of the carboxyl-terminal domain of CaM to the Ca-ATPase, and K_2 represents the product of the association constants of both domains (i.e., $k_1^2 \times k_{2b}$), where k_{2b} is the apparent association constant for the amino-terminal domain of CaM with the Ca-ATPase, assuming the bulk concentration (b) of the N-terminal domain of CaM bound to the PM Ca-ATPase corresponds to the dissociation constant of the carboxyl-terminal domain (i.e., k_1). An estimate of the actual association constant (k_2) for the amino-terminal domain can be obtained by taking into account the effective concentration of the amino-terminal domain following association of the carboxyl-terminal domain, which equals

$$k_2 = \frac{bk_{2b}}{c} \quad (4)$$

The effective concentration of the amino-terminal domain (c) is approximately 0.4 mM and is calculated as 1 over Avogadro's number multiplied by the volume (V) available to the amino-terminal domain, where

$$c = \frac{1}{N_a V} = \frac{1}{\frac{4}{3}\pi N_a \times \mathrm{length}^3} \quad (5)$$

The overall length of CaM (assumed to be approximately 100 Å after association of the carboxyl-terminal domain) is used to define the radius of the volume element available to the amino-terminal domain.

Calculation of Calcium Binding Parameters. To explicitly analyze for the relative affinities and cooperative interactions between the individual calcium binding sites, data was fit to the equation

$$\text{activity} = \frac{K_1[\mathrm{Ca}^{2+}]_{\mathrm{free}} + 2K_2[\mathrm{Ca}^{2+}]^2_{\mathrm{free}}}{2(1 + K_1[\mathrm{Ca}^{2+}]_{\mathrm{free}} + K_2[\mathrm{Ca}^{2+}]^2_{\mathrm{free}})} \quad (6)$$

where $[Ca^{2+}]_{free}$ corresponds to the concentration of unbound calcium, K_1 is the macroscopic equilibrium constant that corresponds to the sum of the intrinsic equilibrium constants (k_1 and k_2) associated with ligand binding to the two classes of binding sites, and K_2 represents the intrinsic equilibrium constant for binding ligand to both classes of ligand binding sites ($k_1k_2k_c$), where k_c provides a quantitative estimate of the lower limit with respect to the cooperative interactions between the sites (*30*).

Circular Dichroism Spectroscopy. Circular dichroism (CD) spectra were measured using a Jasco J-710 spectropolarimeter (Jasco Corp., Tokyo, Japan) and a temperature-jacketed

spectral cell with a path length of 1.0 cm. Spectra were recorded at 1 nm intervals between 200 and 240 nm at 20 °C for desalted apo-CaM and calcium-saturated CaM (50 μg/mL) in 20 mM Tris-HCl (pH 7.5) and either 0.1 mM EGTA or 0.1 mM $CaCl_2$ in the absence and presence of 0.1 M KCl. The apparent α-helical content was determined using the method of ridge regression (*54*), using the computer program Contin (*55, 56*).

Fluorescence Measurements. Steady-state or frequency-domain lifetime and anisotropy measurements involved either the 333 nm output from a Coherent Innova 400 argon ion laser (Sant Clara, CA) to excite AEDANS or tripled output (297 nm) of a Ti:sapphire laser (Coherent, Mira 900) tuned to 891 nm, whose frequency was reduced to 5 MHz using a Coherent pulse picker (model 9200) to excite tryptophan. The CW output (333 nm) or the harmonic content contained within the pulse train generated by the Ti:sapphire laser (297 nm) was used to measure the fluorescence lifetime or anisotropy of AEDANS and Trp, respectively. The design of this instrument has been described in detail elsewhere (*57, 58*). The emitted fluorescence intensity for lifetime or anisotropy measurements of Trp or AEDANS was respectively detected subsequent to a monochromator centered at 346 nm (8 nm band-pass) or a Schott long-pass GG400 filter.

Analysis of Frequency-Domain Data. The time-dependent decay $I(t)$ of any fluorophore can be described as a sum of exponentials:

$$I(t) = \sum_{i=1}^{n} \alpha_i e^{-t/\tau_i} \tag{7}$$

where α_i are the preexponential factors, τ_i are the excited-state decay times, and n is the number of exponential components required to describe the decay. Explicit expressions have been provided that permit the ready calculation of α_i and τ_i (*59*). The parameter values were determined by minimizing the χ^2_R (the *F*-statistic), which serves as a goodness-of-fit parameter that provides a quantitative comparison of the adequacy of different assumed models (*60*). Data were fit using the method of nonlinear least squares to a sum of exponential decays (*61*). After the measurement of the intensity decay, one typically calculates the mean lifetime, $\bar{\tau}$, which is weighted by the amplitudes associated with each of the preexponential terms, where

$$\bar{\tau} = \sum_{i=1}^{n} \alpha_i \tau_i \tag{8}$$

and $\bar{\tau}$ is directly related to the quantum yield of the fluorophore (*62*). Alternatively, to determine the bimolecular quenching efficiency, the average lifetime ($\langle\tau\rangle$) provides a measure of the time that the excited state is available for quenching, where

$$\langle\tau\rangle = \sum_{i=1}^{n} \alpha_i \tau_i^2 / \sum_{i=1}^{n} \alpha_i \tau_i \tag{9}$$

For the case of fluorescence resonance energy transfer (FRET) measurements, more realistic physical models were used involving a distribution of distances (see below), as previously described (*6, 63, 64*).

Calculation of Molecular Distances Using FRET. The efficiencies of energy transfer, E, and the apparent donor−acceptor distance, r_{app}, are calculated from the Förster equations (*65*), where

$$E = 1 - \frac{F_{da} - F_d(1 - f_a)}{F_d f_a} = 1 - \frac{\bar{\tau}_{da} - \bar{\tau}_d(1 - f_a)}{\bar{\tau}_{da} f_a} = \frac{R_0^6}{R_0^6 + r^6} \tag{10}$$

F_{da} and F_d or $\bar{\tau}_{da}$ and $\bar{\tau}_d$ are the steady-state fluorescence intensities and mean fluorescence lifetimes of Trp^{99} in the presence and absence of the FRET acceptor AEDANS. R_0 is the Förster critical distance that defines the distance for a given donor−acceptor pair where the efficiency of FRET is 50%. f_a is the fractional labeling of the acceptor. R_0 is the Förster distance where $E = 0.50$ and is given by

$$R_0 = (9.79 \times 10^{-5})(n^{-4}\kappa^2\phi_d J)^{1/6} \quad \text{(in cm)} \tag{11}$$

where n is the refractive index, κ^2 is the orientation factor, J is the overlap integral, and ϕ_d is the quantum yield of the donor in the absence of acceptor. In our experiments, n is estimated to be 1.40 (*65*); κ^2 is $^2/_3$, which assumes that donor and acceptor chromophores undergo rapid isotropic rotational motion compared with the lifetime of the donor (see below); ϕ_d is determined by numerical integration of the fluorescence emission spectrum of Trp^{99} in CaM, using L-tryptophan in 20 mM MOPS (pH 7.0) as a standard, which has a quantum yield of 0.14 (*66*); and J is calculated by numerical integration from the fluorescence emission spectrum of Trp^{99} in CaM and the absorption spectrum of AEDANS bound to Cys^{69} in CaM. Color effects relating to the wavelength-dependent properties of the photomultiplier were corrected using an algorithm provided by ISS Inc. (Urbana-Champaign, IL). In the presence of saturating calcium (pH 7.5), the quantum yield (ϕ_d) for Trp^{99} is 0.098, and the overlap integral, J, for Trp^{99} to AEDANS bound to Cys^{69} is 9.0×10^{-15} M^{-1} cm^3. These constants were remeasured under the different experimental conditions used in this study and are reflected in the measured values of R_0 (Table 1).

The above analysis assumes a unique donor−acceptor separation in the calculation of molecular distances and ignores any conformational heterogeneity associated with the molecular dynamics of CaM. However, the intensity decay associated with the donor in the presence of an acceptor permits one to recover the conformational heterogeneity (or distribution of distances) associated with CaM (*63, 67, 68*). If a single acceptor is present at a distance r from a donor, then the transfer rate is given by

$$k_{T_i} = \frac{1}{\tau_{D_i}} \left(\frac{R_0}{r}\right)^6 \tag{12}$$

where R_0 is the Förster distance. If a single D−A pair is separated by a fixed distance, r, the intensity decay is given by

$$I_{DA}(r,t) = \sum_{i=1}^{n} \alpha_{D_i} \exp(-t/\tau_{DA_i}) \tag{13}$$

where the individual decay times observed in the presence

Table 1: Spatial Separation between Trp[99] and AEDANS Bound to Cys[69] [a]

exptl conditions[b]	ligand	E[c] (%)	R_0[d] (Å)	r_{app}[e] (Å)	R_{av}[f] (Å)	HW[f] (Å)	χ^2_R[g]
pH 7.5 + 0.1 M KCl	+calcium	15 ± 3%	22.6 ± 0.1	30 ± 1	31 (30−32)	<10	1.8
	+EGTA	7 ± 1%	23.8 ± 0.1	37 ± 2	38 (37−43)	<16	2.1
pH 7.5 (no KCl)	+calcium	10 ± 3%	22.5 ± 0.1	32 ± 2	33 (32−37)	7 (1−16)	0.8
	+EGTA	24 ± 3%	23.4 ± 0.1	28 ± 1	4 (1−14)	43 (30−51)	2.1
pH 6.3 + 0.1 M KCl	+calcium	18 ± 3%	22.8 ± 0.1	29 ± 1	31 (30−32)	9 (2−14)	1.0
	+EGTA	11 ± 2%	23.8 ± 0.1	33 ± 1	36 (34−37)	14 (9−18)	1.0
pH 5.0 + 0.1 M KCl	+calcium	22 ± 4%	22.2 ± 0.1	27 ± 1	26.7 (26.4−27.1)	<7	2.1
	+EGTA	27 ± 3%	22.8 ± 0.1	27 ± 1	26.1 (25.8−26.4)	14 (12−16)	1.1

[a] Values and associated errors were obtained from seven to ten independent measurements of FRET between Trp[99] and AEDANS bound to Cys[69]. [b] Experimental conditions include 3 μM CaM in 0.1 mM EGTA and when indicated either 0.2 mM $CaCl_2$ (pH 7.5) or 0.6 mM $CaCl_2$ (pH 6.3 and 5.0) in the presence of either 0.1 M HEPES (pH 7.5), 0.1 M MES (pH 6.3), or 0.1 M HOMOPIPES (pH 5.0). [c] Energy transfer efficiencies (E) for lifetime-resolved measurements of Trp[99] represent average values and associated standard errors of the mean, as described in Experimental Procedures (eq 10). [d] Förster critical distance (R_o) under the indicated experimental conditions. [e] Apparent distance between Trp[99] and AEDANS bound to Cys[69] calculated from eq 10 assuming a unique conformation. [f] Average donor−acceptor distance (R_{av}) or full width at half-maximum (HW) assuming a Gaussian distribution of distances (*63*, *68*). Indicated errors were obtained from a global analysis of errors, as depicted in Figure 5. [g] Average value of reduced chi-squared (χ^2_R) fit to Gaussian distribution of distances.

of the energy transfer acceptor are

$$\frac{1}{\tau_{DA_i}} = \frac{1}{\tau_{D_i}} + \frac{1}{\tau_{D_i}}\left(\frac{R_0}{r}\right)^6 \tag{14}$$

One generally does not observe a unique D−A separation in biomolecules but rather an average determined by the probability distance distribution P(r) (*68*). A distribution of D−A separations is expected from measurements of molecular dynamics of a range of proteins, as well as statistic mechanical simulations that indicate the presence of conformational heterogeneity associated with long polymers (*60*). The latter calculations indicate that long polymers can be adequately described using Gaussian distribution functions. Hence, the observed intensity decay is

$$I_{DA}(t) = \int_{r=0}^{\infty} P(r)\sum_{i=1}^{n}\alpha_{D_i}\exp\left[-\frac{t}{\tau_{D_i}} - \frac{t}{\tau_{D_i}}\left(\frac{R_0}{r}\right)^6\right] dr \tag{15}$$

It should be noted that the proper choice of boundary conditions ensures the elimination of negative distances (i.e., $r < 0$), which are physically unrealistic. Therefore, if part of the Gaussian distribution [$P(r)$] contains distances less than 0, then the integral [i.e., $\int P(r)\, dr$] is less than unity. This type of truncated Gaussian distance distribution has previously been applied to staphylococcal nuclease, melittin, thiopeptides, and denatured troponin I (*64*, *69*−*71*).

Our objective is to recover $P(r)$ from the intensity decay. To minimize the number of parameters, a uniform Gaussian distribution of donor to acceptor distances is generally assumed:

$$P(r) = \exp\left[-\frac{1}{2}\left(\frac{r - R_{av}}{\sigma}\right)^2\right] \tag{16}$$

where R_{av} is the average distance and σ is the standard deviation of the distribution. The width of the distribution is reported as the full width at half-maximum (half-width, hw), which is given by hw = 2.354σ. For analysis in terms of a sum of exponentials, we used the analytical forms of N_ω and D_ω previously described (*58*−*60*), using the Globals software package (University of Illinois, Urbana-Champaign). For the distance distributions we used numerical integration to calculate

$$N_\omega = \int_{r=0}^{\infty}\sum_{i=0}^{n}\frac{P(r)\omega\tau_{DA_i}^2}{1+\omega^2\tau_{DA_i}^2}\, dr$$
$$D_\omega = \int_{r=0}^{\infty}\sum_{i=1}^{n}\frac{P(r)\tau_{DA_i}}{1+\omega^2\tau_{DA_i}^2}\, dr \tag{17}$$

using software provided by the Center for Fluorescence Spectroscopy (Baltimore, MD). The adequacy of the Gaussian model is assessed through a comparison of the goodness of the fit (i.e., χ^2_R; see below) relative to the fit using the more general multiexponential model, which assumes no physical model.

Decays of Fluorescence Anisotropy. As previously described, time-resolved anisotropies were measured using the differential phase ($\Delta_\omega = \phi_\perp - \phi_{||}$) and modulated anisotropy ($r_\omega = [\Lambda_\omega - 1]/[\Lambda_\omega + 2]$), where $\Lambda = m_{||}/m_\perp$(*60*, *72*). The parameters describing the anisotropy decay were obtained from a least-squares fit to a multiexponential model, where

$$r(t) = r_0\sum_{i=1}^{n} g_i e^{-t/\phi_i} \tag{18}$$

r_0 is the limiting anisotropy in the absence of rotational diffusion, ϕ_i are the rotational correlation times, $r_0 g_i$ are the amplitudes of the total anisotropy loss associated with each rotational correlation time, and n is the total number of components associated with the exponential decay. The goodness of fit was determined through a comparison of the deviations between the measured and calculated values. Errors in Δ_ω and Λ_ω were assumed to be 0.2 and 0.005, respectively.

RESULTS

Construction and Chemical Modification of a CaM Mutant for Fluorescence Measurements. Using site-directed mutagenesis to introduce conservative amino acid substitutions involving Leu[69] → Cys[69] and Tyr[99] → Trp[99] (Figure 1), it is possible to use fluorescence spectroscopy to measure the conformation and dynamics of the central helix in CaM (*68*). Using DTNB to titrate the thiol content in CaM, there is

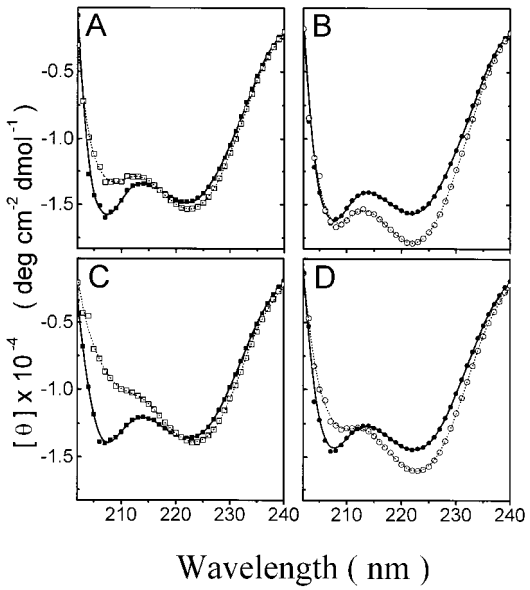

FIGURE 2: Sensitivity of CaM secondary structure to ionic strength. Circular dichroism spectra for apo-CaM (A, C) or calcium-saturated CaM (B, D) in the presence of either 0.1 mM EGTA (□, ■) or 0.1 mM $CaCl_2$ (○, ●) in the absence (□, ○) or presence (■, ●) of 0.1 M KCl using wild-type CaM (A, B) or CaMCW (C, D), which contains the site-directed substitution of $Leu^{69} \rightarrow Cys^{69}$ and $Tyr^{99} \rightarrow Trp^{99}$. CaM concentration was 50 μg/mL. Symbols correspond to experimental data, and lines represent nonlinear least-squares fits. The calculated α-helical content in the absence and presence of 0.1 M KCl for apo-CaM was respectively 48 ± 2% and 59 ± 3% for CaM and 53 ± 3% and 63 ± 3% for CaMCW. The calculated α-helical content in the absence and presence of 0.1 M KCl for calcium-saturated CaM was respectively 62 ± 4% and 67 ± 3% for CaM and 56 ± 3% and 66 ± 3% for CaMCW.

0.95 ± 0.05 mol of cysteine/mol of CaM. These results indicate that following the reduction and purification of CaM there are essentially no disulfide cross-linkages between CaM molecules. Thus, upon covalent modification of Cys^{69} with a suitable chromophore (i.e., AEDANS) whose absorbance spectrum overlaps the fluorescence emission of Trp^{99}, one can use Trp^{99} as a fluorescence resonance energy transfer (FRET) donor (D) to measure the spatial separation between Trp^{99} and Cys^{69}, at the opposing ends of the central helix in CaM.

Comparison of Wild-Type and Genetically Engineered CaM. To detect possible alterations in the secondary structure of CaM that might result from the site-directed substitution of $Leu^{69} \rightarrow Cys^{69}$ and $Tyr^{99} \rightarrow Trp^{99}$, we have used CD spectroscopy to compare the average α-helical content in wild-type and mutant CaM. There are no significant differences in the secondary structures of wild-type or mutant CaM (Figure 2), which respectively were found to contain approximately 67 ± 3% and 66 ± 3% α-helical content following calcium activation in the presence of 0.1 M KCl. Additional resolution of possible structural differences between wild-type and genetically engineered CaM, which may result from either the introduction of site-directed amino acid substitutions (see above) or the attachment of AEDANS to Cys^{69}, involved the comparison of the CaM and calcium dependence of the activation of the PM Ca-ATPase by wild-type and mutant CaM. Using either wild-type CaM or a site-specific mutant CaM labeled at Cys^{69} with IAEDANS, there is an equivalent 3-fold activation of the PM Ca-ATPase upon addition of saturating concentrations of CaM and calcium

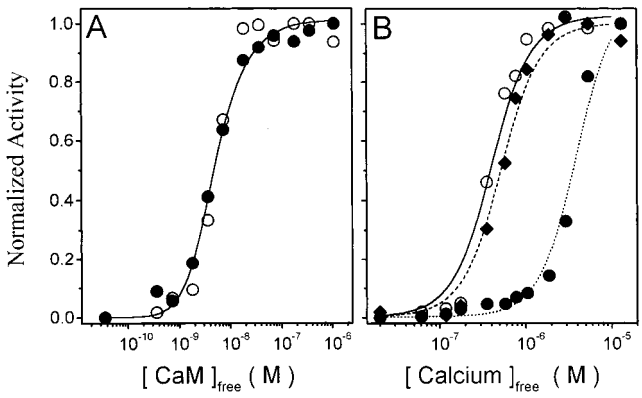

FIGURE 3: Comparison of wild-type and mutant CaM to activate the PM Ca-ATPase. Rates of ATP hydrolysis for the PM Ca-ATPase in porcine erythrocyte ghosts in the presence of either (A) 30 μM free calcium or (B) 0.3 μM CaM for wild-type CaM (○), $CaMC^{69}W^{99}$ (◆), or AEDANS-labeled $CaMC^{69}W^{99}$ (●). ATPase activity was measured at 37 °C after the addition of 5 mM ATP into a reaction mixture containing 0.4 mg ml^{-1} porcine erythrocyte ghost protein in 25 mM HEPES (pH 7.5), 0.1 M KCl, 6 mM $MgCl_2$, 3 μM A23187, the indicated concentration of CaM, and sufficient calcium to yield the desired free calcium concentration. The concentrations of wild-type (○) or AEDANS-modified (●) CaM necessary for half-maximal activation of the PM Ca-ATPase are 5.1 ± 0.3 nM and 4.8 ± 0.3 nM, respectively (panel A). A least-squares fit to both data sets using eq 2 in Experimental Procedures indicates that the association constants (i.e., k_1 and k_2) for the carboxyl- and amino-terminal domains of CaM are (1.0 ± 0.1) × 10^8 M^{-1} and (1 ± 1) × 10^5 M^{-1}, respectively. The concentrations of calcium necessary for half-maximal activation of the PM Ca-ATPase in the presence of saturating CaM concentrations are 0.4 ± 0.1 μM (○), 0.5 ± 0.1 μM (◆), and 3.7 ± 0.2 μM (●), respectively (panel B). Fitting these data to eq 6 indicates that $\Delta G_1 = -7.3 \pm 0.7$ kcal mol^{-1}, $\Delta G_2 = -17.1 \pm 0.1$ kcal mol^{-1}, and $\Delta G_c = -3.4 \pm 0.7$ kcal mol^{-1} (○); $\Delta G_1 = -7.5 \pm 0.7$ kcal mol^{-1}, $\Delta G_2 = -17.4 \pm 0.1$ kcal mol^{-1}, and $\Delta G_c = -3.2 \pm 0.7$ kcal mol^{-1} (◆); and $\Delta G_1 = -5.7 \pm 0.9$ kcal mol^{-1}, $\Delta G_2 = -14.7 \pm 0.1$ kcal mol^{-1}, and $\Delta G_c = -4.2 \pm 0.9$ kcal mol^{-1} (●). The concentration of unbound (free) CaM was determined using eq 1 in Experimental Procedures. Free calcium concentrations were calculated as previously described (*94*).

(Figure 3). The virtually identical CaM dependence of activation indicates that wild-type and AEDANS-labeled CaM undergo analogous binding interactions with the PM Ca-ATPase (Figure 3A), suggesting that the structure of calcium-activated CaM bound to the PM Ca-ATPase is not altered. While these site-directed mutations and subsequent covalent attachment of AEDANS do modify the calcium dependence of CaM-activation of the PM Ca-ATPase, there is no alteration in the cooperativity of calcium activation (see legend in Figure 3B). Thus, the introduction of Trp^{99} and Cys^{69}, and the modification of Cys^{69} with IAEDANS, does not alter the structural coupling between CaM and the PM Ca-ATPase. These results indicate that we can use this fluorescently labeled CaM derivative to assess the structure and dynamics of the central helix under physiological conditions.

Sensitivity of the Secondary Structure of CaM to Changes in Ionic Strength. Calcium activation results in minor changes in the CD spectra of CaM in the presence of 0.1 M KCl, consistent with earlier suggestions that calcium binding primarily results in a reorientation of secondary structural elements with respect to one another (*2*−*5*). In contrast, the CD spectra of apo-CaM and calcium-activated CaM are different in the presence and absence of 0.1 M KCl (Figure

2). Upon increasing the ionic strength, the ratio of the molar ellipticities at 208 and 222 nm (i.e., $\theta_{208}/\theta_{222}$) increases for apo-CaM and decreases for calcium-activated CaM, consistent with previous suggestions that the structure of CaM is affected by changes in monovalent ion concentrations (*27*, *73*, *74*). Consistent with the observed spectral changes, fitting the experimental data suggests that addition of 0.1 M KCl results in a 9% increase in the average α-helical content of CaM. These results indicate that the structure of CaM determined at low ionic strength may not represent a unique structure of CaM in solution (*12*, *13*) and suggests a need to consider the structure of CaM at the higher ionic strengths characteristic of cellular conditions.

Calcium-Dependent Alterations in the Structure of the Central Helix. To identify possible calcium-dependent alterations in the average conformation of the central helix, the steady-state emission spectra and fluorescence lifetime parameters of tryptophan in apo-CaM and calcium-activated CaM were measured in the absence and presence of the FRET acceptor AEDANS (Figure 4). Under these conditions AEDANS is not directly excited to any appreciable extent. Therefore, the decrease in the steady-state fluorescence intensity of Trp^{99} and the large increase in the stimulated emission of AEDANS are due to FRET (*65*). From the steady-state spectra, one observes that upon calcium activation the amount of FRET between Trp^{99} and AEDANS bound to Cys^{69} increases from 5 ± 1% to about 13 ± 2%. This change in FRET can be used to calculate changes in the apparent spatial separation between these chromophores that result from calcium activation of CaM (see eq 10 in Experimental Procedures). Thus, on the basis of these *steady-state* measurements the apparent spatial separation (r_{app}) between Trp^{99} and AEDANS (bound to Cys^{69}) decreases 6 ± 2 Å from 37 ± 2 Å in apo-CaM to 31 ± 1 Å upon calcium activation of CaM. This result suggests that there is a direct structural coupling between the opposing globular domains in CaM and that calcium activation alters the structure of the central helix.

Complementary information regarding the average structure and conformational heterogeneity of the central helix is available from a consideration of the time-dependent decay of the Trp^{99} in the absence and presence of AEDANS. In the presence of AEDANS the frequency response of both apo-CaM and calcium-saturated CaM is shifted toward higher frequencies (Figure 4C,D), indicating that the average lifetime is shorter due to the presence of FRET. The intensity decay of Trp^{99} can be adequately described as a sum of three exponentials, as indicated by the random distribution of the weighted residuals about the origin. Inclusion of additional fitting parameters results in no further improvement of χ^2_R (see legend to Figure 4). The average amount of FRET calculated from the reduction in the mean fluorescence lifetime ($\bar{\tau}$) of Trp^{99} increases from 7 ± 1% to 15 ± 3% upon calcium activation (Table 1), which is comparable to that calculated from steady-state measurements (see above). Thus, the sample is homogeneous and contains no significant population of fluorophores whose spatial separation between Trp^{99} and AEDANS at Cys^{69} is less than $0.5R_0$, which would result in a static component of FRET that would selectively decrease the steady-state fluorescence intensity without altering the average lifetime (*75*). These latter results agree with earlier NMR measurements, which also indicate that the opposing globular domains in CaM do not come into direct contact (*13*). Thus, the time-dependent decrease in the fluorescence intensity decay of Trp^{99} resulting from FRET to AEDANS at Cys^{69} can be used to recover the conformational heterogeneity of the central helix, which typically involves fitting the data to a model that assumes a Gaussian distribution of distances between donor and acceptor chromophores (*6*, *63*, *68*, *76*). The similar goodness of fit (i.e., χ^2_R) obtained when the lifetime data are fit to a model that assumes a Gaussian distribution of distances with two floating parameters (i.e., R_{av} and HW; Table 1) in comparison to the fit obtained using a sum of exponentials with five

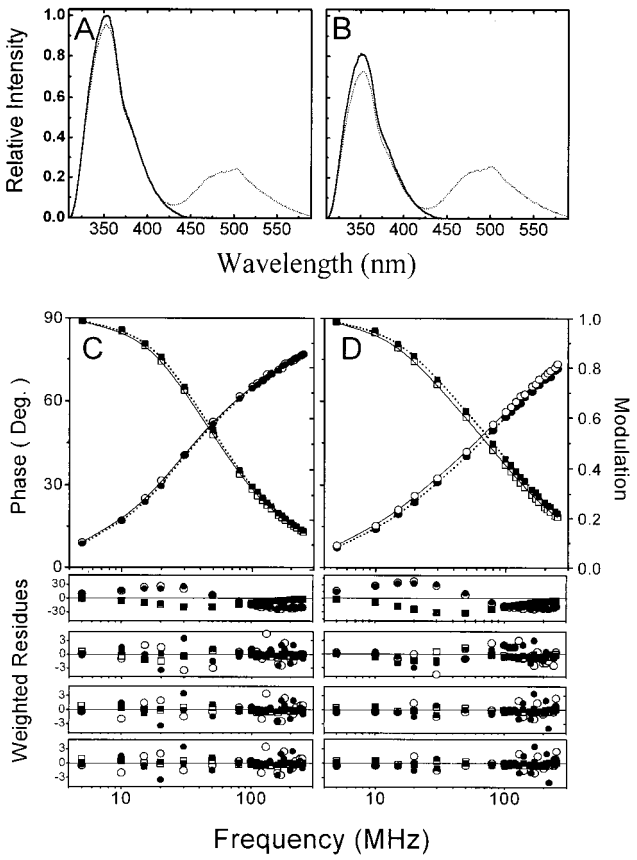

FIGURE 4: Steady-state and fluorescence lifetime data for CaM. Steady-state (A and B) and frequency-response (C and D) data for Trp^{99} (donor) in the absence (solid line) and presence (dotted line) of the FRET acceptor AEDANS for apo-CaM (A and C) and calcium-saturated CaM (B and D). In the case of the frequency-domain fluorescence lifetime data, the phase shift (○, ●) or modulation (□, ■) is shown for Trp^{99} in the absence (○, □) and presence (●, ■) of the FRET acceptor AEDANS. Symbols represent the experimental data, and lines represent a three-exponential fit to the data. Weighted residues are shown below the data (from top to bottom) for the one-, two-, three-, and four-component fit to the data, where frequency-independent errors in the phase and modulation were assumed to be 0.2° and 0.005, respectively. The respective χ^2_R values for Trp^{99} in apo-CaM in the absence and presence of AEDANS are 240 and 212 (one-component fit), 1.8 and 1.7 (two-component fit), 1.5 and 1.5 (three-component fit), and 1.5 and 1.5 (four-component fit). The respective χ^2_R values for Trp^{99} in calcium-saturated CaM in the absence and presence of AEDANS are 400 and 381 (one-component fit), 3.3 and 3.4 (two-component fit), 1.6 and 2.2 (three-component fit), and 1.6 and 2.2 (four-component fit). Measurements involved 3 μM CaM in 0.1 M HEPES (pH 7.5), 0.1 M KCl, 0.1 mM EGTA, and when appropriate 0.2 mM $CaCl_2$. The molar ratio of AEDANS bound to CaM was 0.70 ± 0.02. Excitation was 297 nm, and emission was detected subsequent to a monochromator centered at 346 nm (8 nm band-pass) for the lifetime data. The temperature was 20 °C.

Table 2: Lifetime Data for Trp^{99} in the Absence and Presence of the FRET Acceptor AEDANS Bound to Cys^{69} [a]

exptl conditions[b]	ligand	label	α_1	τ_1 (ns)	α_2	τ_2 (ns)	α_3	τ_3 (ns)	$\bar{\tau}$ (ns)	χ^2_R[c]
pH 7.5 + 0.1 M KCl	+calcium	donor	0.39	1.3	0.45	2.6	0.16	8.0	2.9	1.6
			(0.08)	(0.1)	(0.05)	(0.3)	(0.03)	(0.5)	(0.1)	
		D−A	0.44	1.2	0.41	2.5	0.15	7.3	2.6	1.6
			(0.03)	(0.1)	(0.02)	(0.1)	(0.01)	(0.3)	(0.1)	
	+EGTA	donor	0.27	1.1	0.23	3.2	0.50	5.9	4.0	1.5
			(0.04)	(0.1)	(0.07)	(0.1)	(0.03)	(0.1)	(0.1)	
		D−A	0.29	1.1	0.30	3.8	0.41	5.8	3.8	1.5
			(0.01)	(0.1)	(0.02)	(0.2)	(0.01)	(0.1)	(0.1)	
pH 7.5 (no KCl)	+calcium	donor	0.80	1.8			0.20	7.0	2.8	2.3
			(0.01)	(0.1)			(0.01)	(0.1)	(0.1)	
		D−A	0.79	1.6			0.21	6.4	2.6	1.0
			(0.01)	(0.1)			(0.01)	(0.1)	(0.1)	
	+EGTA	donor	0.39	1.5			0.61	4.9	3.6	2.8
			(0.02)	(0.1)			(0.02)	(0.1)	(0.1)	
		D−A	0.42	1.0			0.58	4.4	3.0	3.8
			(0.01)	(0.1)			(0.01)	(0.1)	(0.1)	
pH 6.3 + 0.1 M KCl	+calcium	donor	0.31	1.3	0.47	2.4	0.22	6.9	3.1	1.0
			(0.03)	(0.1)	(0.03)	(0.1)	(0.01)	(0.1)	(0.1)	
		D−A	0.40	1.2	0.42	2.5	0.17	6.7	2.7	0.8
			(0.04)	(0.1)	(0.03)	(0.2)	(0.01)	(0.1)	(0.1)	
	+EGTA	donor	0.21	1.1	0.26	2.7	0.53	5.7	3.9	2.1
			(0.04)	(0.1)	(0.05)	(0.6)	(0.08)	(0.2)	(0.1)	
		D−A	0.21	1.1	0.19	2.0	0.59	5.1	3.6	1.0
			(0.04)	(0.1)	(0.02)	(0.5)	(0.03)	(0.1)	(0.1)	
pH 5.0 + 0.1 M KCl	+calcium	donor	0.36	1.3	0.46	2.1	0.18	6.6	2.6	1.4
			(0.01)	(0.1)	(0.02)	(0.1)	(0.01)	(0.1)	(0.1)	
	+EGTA	D−A	0.30	0.9	0.56	1.9	0.14	6.0	2.2	1.0
			(0.03)	(0.1)	(0.03)	(0.1)	(0.01)	(0.1)	(0.1)	
		donor	0.33	1.3	0.26	2.1	0.41	5.2	3.1	1.3
			(0.01)	(0.1)	(0.01)	(0.1)	(0.01)	(0.1)	(0.1)	
		D−A	0.36	0.9	0.38	2.1	0.27	5.0	2.5	0.8
			(0.02)	(0.1)	(0.02)	(0.1)	(0.01)	(0.1)	(0.1)	

[a] Indicated values and associated standard errors of the mean (in parentheses) for seven to ten independent measurements were obtained from a two- or three-exponential fit to frequency-domain data collected for Trp^{99} in the absence (donor) or presence (D−A) of AEDANS bound to Cys^{69}, as described in Experimental Procedures (see eqs 7 and 8). [b] Experimental conditions are as described in Table 1. [c] χ^2_R is the average value of the reduced chi squared. The fractional labeling of Cys^{69} with AEDANS was 0.70.

floating parameters (i.e., α_1, τ_1, α_2, τ_2, and τ_3; Table 2) indicates that fitting the data to the simpler model involving a distribution of distances is statistically justifiable.

The average donor−acceptor separations (R_{av}) between Trp^{99} and AEDANS bound to Cys^{69} for apo-CaM and calcium-activated CaM obtained from these lifetime measurements are 38 and 31 Å, respectively (Table 1). These values are very similar to the apparent donor−acceptor separation calculated by assuming a single unique conformation for both apo-CaM ($r_{app} = 37 \pm 2$ Å) or calcium-activated CaM ($r_{app} = 30 \pm 1$ Å), consistent with the relatively narrow half-width of the Gaussian distance distribution (Figure 5B; Table 1). A consideration of the error surfaces for these calculated distance distributions provides a conservative estimate of the recovered parameters (*67*, *77*), and demonstrates the presence of two well-defined conformations for the central helix in apo-CaM and calcium-activated CaM that are conformationally distinct (Figure 5A). Thus, the 7 ± 2 Å decrease in the average distance (R_{av}) between Trp^{99} and AEDANS at Cys^{69} is the result of a conformational change between two unique conformations, which are modulated by calcium binding.

Ionic Strength or pH Alters the Structure of the Central Helix. The identification of defined conformations for the central helix in apo-CaM and calcium-activated CaM is in marked contrast to earlier results, which suggest that the central helix is disordered under solution conditions and that the opposing globular domains of CaM undergo essentially uncoupled rotational motion with respect to one another (*12*, *13*). Since these previous solution measurements have emphasized conditions involving low ionic strength and acidic pH, it is of interest to consider whether these differences may modulate the structure of the central helix. We have therefore measured the fluorescence intensity decay of Trp^{99} in the absence and presence of AEDANS bound to Cys^{69}, located on opposite sides of the central helix, under a range of solution conditions (Figure 6). At low ionic strength (pH 7.5) the intensity decay of Trp^{99} can be adequately described by two-exponential components and is markedly different from that observed in the presence of 100 mM KCl (Table 2). These results indicate that the environment around Trp^{99} in calcium binding loop 2 is sensitive to changes in ionic strength. Using FRET to measure the spatial separation between Trp^{99} and AEDANS bound to Cys^{69} at low ionic strength, one observes that calcium activation results in a reduction in the FRET efficiency (Figure 6C,D; Table 1). Thus, in contrast to the calcium-dependent decrease in the average spatial separation between Trp^{99} and AEDANS (pH 7.5, 0.1 M KCl), at low ionic strength calcium results in an increase in the average spatial separation between these donor and acceptor chromophores. A consideration of the recovered distribution of distances further indicates that there is considerably more conformational heterogeneity for apo-CaM at low ionic

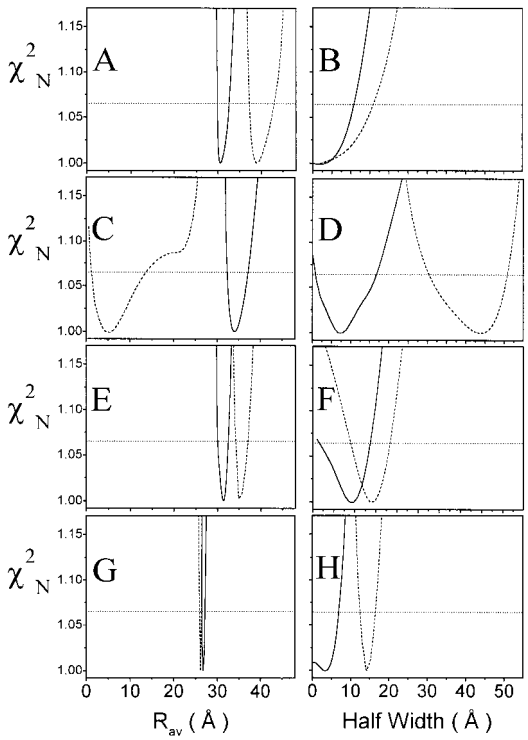

FIGURE 5: Depiction of error surfaces for the Gaussian distance distribution model. Parameter values were obtained from a simultaneous fit using 7−10 data sets to recover the average spatial separation (R_{av}) and half-Width for a model involving a Gaussian distribution of distance between Trp[99] and AEDANS covalently linked to Cys[69] for apo-CaM (dashed line) and calcium-saturated (solid line) CaM at pH 7.5 in the presence (A, B) and absence (C, D) of 0.1 M KCl, at pH 6.3 in the presence of 0.1 M KCl (E, F), or at pH 5.0 in the presence of 0.1 M KCl (G, H). Experimental values (i.e., R_{av} or half-width) were incrementally adjusted, and all other parameters were allowed to vary in the least-squares analysis, essentially as previously described (*77*). The horizontal line corresponds to the *F*-statistic for one standard deviation. Experimental conditions are as described in the legend to Table 1.

strength, as indicated by the substantially larger half-widths in comparison to those observed in the presence of 100 mM KCl (Figure 5C,D; Table 1). These results suggest the loss of stabilizing interactions within the central helix at low ionic strength and that calcium binding under these conditions results in large structural changes that function to stabilize the structure of the central helix.

One observes that the structures of the central helix for both apo-CaM and calcium-activated CaM at pH 5.0 (100 mM KCl) are different from that observed at pH 7.5, irrespective of ionic strength (Table 1). At this acidic pH calcium binding reduces the conformational heterogeneity of the central helix but results in little change in the average spatial separation between these chromophoric groups (Figure 5G,H). In contrast, the structures of the central helix for both apo-CaM and calcium-activated CaM are virtually identical at pH 6.3 and 7.5 (100 mM KCl), indicating that the change in structure at pH 5.0 is probably the result of the titration of an acidic moiety (such as a carboxylate). Thus, under conditions of low ionic strength or pH the structure of the central helix is altered relative to that observed under physiological conditions. Taken together, these results indicate that the conformation of the central helix is highly dependent on solution conditions and that calcium binding can function to stabilize the structure of the central helix.

Structural Coupling between Opposing Globular Domains. The large increase in the conformational heterogeneity within the central helix of apo-CaM observed at low ionic strengths could be the result of a structural uncoupling between the opposing globular domains in CaM or alternatively may be the result of an increased number of distinct conformations that interconvert on a time scale that is slow compared with the excited-state lifetime of Trp[99] ($\bar{\tau} \approx 3-4$ ns; Table 2). To investigate the structural coupling between the opposing globular domains, we have measured the rotational motion of CaM covalently and specifically labeled with AEDANS bound to Cys[69] (Figure 7). Two rotational correlation times are necessary to describe the data, which are associated with segmental rotational motion ($\phi_1 \approx 2$ ns) and overall protein rotational motion ($\phi_2 \approx 12-13$ ns; Table 3) (*6*). The amplitudes and rotational correlation times are very similar, irrespective of changes in pH or ionic strength (Table 3). Since the longest rotational correlation time of calcium-activated CaM is consistent with the overall hydrodynamic properties of CaM (*6*, *76*), these results indicate that the opposing globular domains remain structurally coupled. Thus, the increased conformational heterogeneity observed at low ionic strength is the result of static disorder between conformational states whose interconversion is slow on the nanosecond time scale. Furthermore, the similar amplitudes and rotational correlation times associated with segmental rotational motion suggest that the tertiary structure surrounding AEDANS is very similar irrespective of the pH or ionic strength. The analogous rotational dynamics of CaM observed in the presence and absence of calcium suggests that calcium binding induces a reorientation of opposing domains with little or no expansion of the central helix, suggesting that the average hydrodynamic structures are comparable.

Possible Errors in the Determination of Molecular Distances. Changes in the apparent Gaussian distance distributions resulting from alterations in pH, ionic strength, or calcium binding could result from distance changes or alterations in the relative orientation (i.e., κ^2) of donor or acceptor chromophores (Table 1). In this study, possible errors in the measurement of molecular distances using FRET were minimized by (i) engineering donor and acceptor chromophoric sites at positions expected to enhance the rates of rotational mobility due to their exposed positions within the crystal structure, which should reduce orientation artifacts (i.e., κ^2 in eq 11), (ii) the use of donor and acceptor chromophores whose Förster distance (R_0) is less than the measured distance (*69*), and (iii) the use of AEDANS as a FRET acceptor, whose multiplicity of absorption transition dipoles further reduces errors arising from orientation effects (*68*). Thus, the large amplitude of the segmental motion of AEDANS, whose rate of motion is fast compared with the global rotational motion of CaM (Table 3), coupled with the large solvent exposure that approaches that of AEDANS free in solution (Table 4), indicates that the measured distance distributions are not appreciably affected by the orientation of AEDANS (*63*). Likewise, Trp[99] undergoes rapid rotational motion ($\phi_1 \approx 1$ ns; Table 5), whose amplitude and rates of motion are relatively insensitive to changes in pH, ionic strength, and calcium binding. Thus, changes in the apparent distance distributions accurately reflect conformational differences and are not the result of changes in the relative orientation of Trp[99] and AEDANS bound to Cys[69]. The

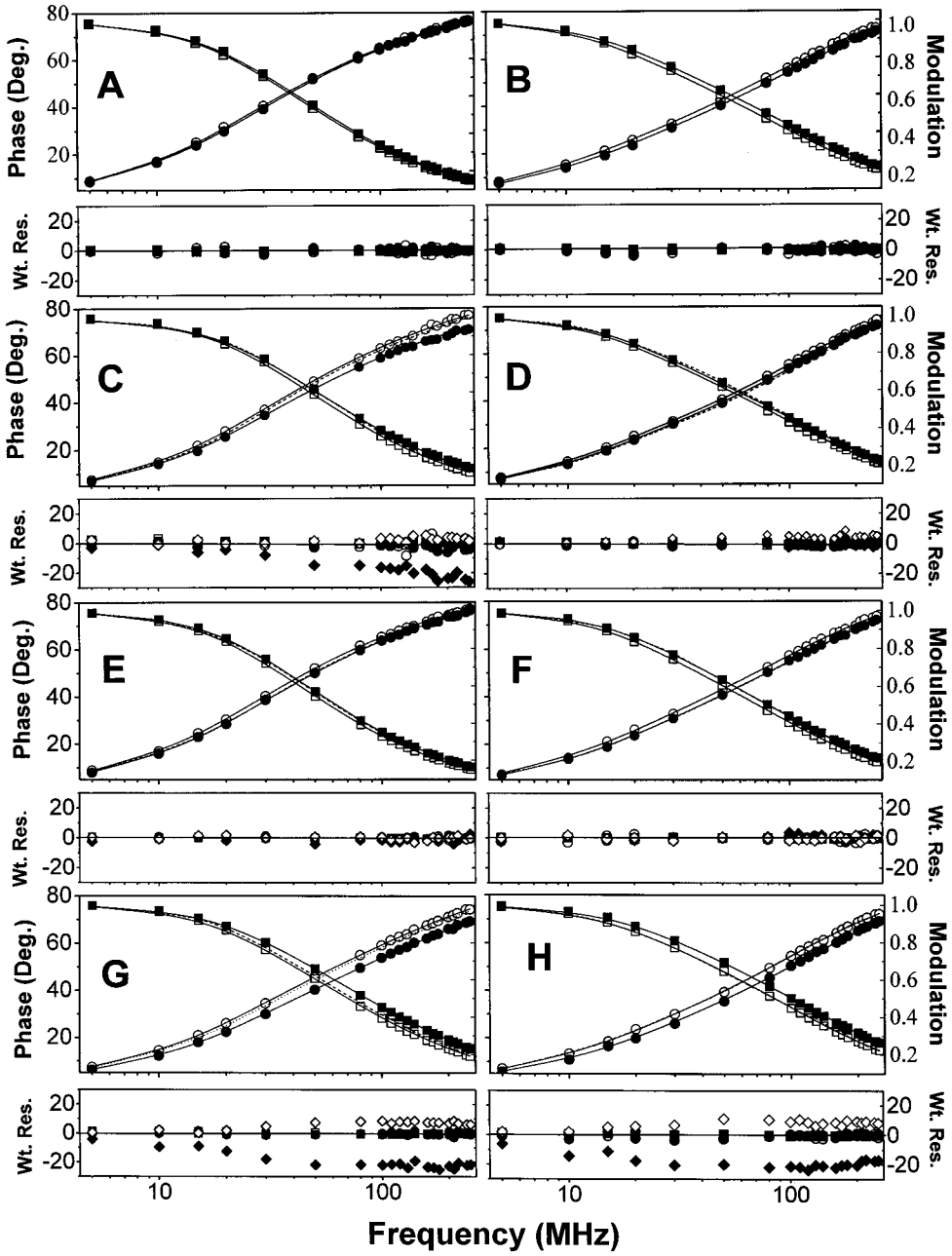

FIGURE 6: Comparison of frequency-domain lifetime data for Trp99 in the absence and presence of the FRET acceptor AEDANS. Phase shift (○, ●) or modulation (□, ■) data for apo-CaM (A, C, E, and G) or calcium-activated CaM (B, D, F, and H) in the absence (○, □) or presence (●, ■) of the FRET acceptor AEDANS. Solid lines represent least-squares fits assuming either a three-exponential fit to the data for donor (○, □) or a distribution of distances (●, ■). Dashed lines represent simulated fits assuming the distance distributions observed in the top panels (0.1 M KCl, pH 7.5). The weighted residuals are shown below the corresponding fits, where the diamond symbols (i.e., ◇ and ◆) represent the simulated fits. The respective χ^2_R values for the least-squares and simulated fits to the distance distrubution model are 1.0 (panel A), 1.2 (panel B), 2.0/139 (panel C), 0.7/12.7 (panel D), 0.8/2.4 (panel E), 0.6/1.2 (panel F), 0.8/223 (panel G), and 1.4/67 (panel H). Measurements involved 3 μM CaM in 0.1 mM EGTA in the absence (panels A, C, E, and G) and presence of either 0.2 mM $CaCl_2$ (panels B and D) or 0.6 mM $CaCl_2$ (panels F and H). Additional buffer conditions involved 0.1 M HEPES (pH 7.5) in the presence (panels A and B) and absence (panels C and D) of 0.1 M KCl, or 0.1 M MES (pH 6.3) (panels E and F), or 0.1 M HOMOPIPES (pH 5.0) (panels G and H) in the presence of 0.1 M KCl.

insensitivity of the rotational dynamics of Trp^{99} and AEDANS to alterations in pH, ionic strength, or calcium binding further indicates that alterations in the distance distribution of the central helix result from localized structural changes that do not appreciably affect the conformation around Trp^{99} or Cys^{69} at the ends of the central helix. Thus, these results are consistent with previous suggestions that $D^{78}-S^{81}$ is conformationally disordered and functions as a flexible hinge element (*7*, *13*, *41*).

DISCUSSION

Summary of Results. We have engineered a fully functional CaM in which the site-directed substitution of $Tyr^{99} \rightarrow Trp^{99}$ and $Leu^{69} \rightarrow Cys^{69}$ permits the investigation of the conformation of the central helix through measurements of FRET between Trp^{99} and AEDANS covalently and selectively bound to Cys^{69} (Figure 1). We observe a narrow distribution of conformations for both calcium-activated CaM and apo-CaM at physiologically relevant ionic strengths (pH 7.5);

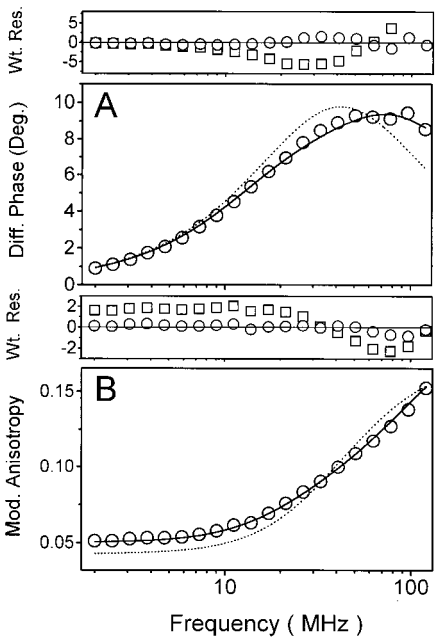

FIGURE 7: Frequency-domain anisotropy data for calcium-activated AEDANS−CaM. The frequency response of the differential phase (A) and modulated anisotropy (B) and the corresponding one- (dotted line) and two-component (solid line) fits to the data are depicted. Weighted residues are shown for one- (□) and two-component (○) fits to the data, whose respective χ^2_R values were 17.7 and 0.6, respectively. Experimental conditions involved 3 μM CaM in 0.1 M HEPES (pH 7.5), 0.1 M KCl, 0.1 mM EGTA, and 0.2 mM $CaCl_2$.

calcium binding results in a 7 ± 2 Å decrease in the average distance, indicating that the central helix adopts structurally distinct conformations for apo-CaM and calcium-activated CaM (Table 1; Figures 5 and 6). The conformation of the central helix is altered at low ionic strength or pH, indicating the presence of ionizable side chains that affect the conformation of CaM. Under all conditions, the opposing globular domains remain structurally coupled, as indicated by the long rotational correlation times ($\phi_2 \approx 12-13$ ns; Table 3) that are consistent with the hydrodynamic structure of a dumbbell-shaped CaM (*6*, *21*). Thus, these results indicate the presence of static disorder within a metastable central helix whose conformation is altered between two distinct conformations by calcium activation.

Relationship to Other Studies. The distance between the C_α carbons in Leu^{69} and Tyr^{99} in the crystal structure of calcium-activated CaM is 37 Å (*11*). Since these side chains face away from one another in the crystal structure, the smaller average distance obtained from FRET measurements of calcium-activated CaM compared with that observed in the crystal structure is therefore consistent with earlier suggestions that the central helix is bent or conformationally disordered in solution (*7*, *13*, *78*, *79*). However, in contrast to earlier NMR results that suggested that the opposing domains of CaM are structurally uncoupled through a flexible linker (*12*, *13*), our results demonstrate the presence of distinct conformations within the central helix in the presence of 0.1 M KCl that are modulated by calcium binding (Figure 5; Table 1). Thus, at physiologically relevant ionic strengths calcium activation functions to alter the relative orientation of the opposing globular domain with respect to each another, which has the potential to affect the kinetics of CaM binding and activation of target proteins. Since changes in ionic strength modulate the conformation of CaM, and the central helix is less stable in the absence of added KCl (Figures 2 and 5), these results suggest that the larger conformational disorder observed using NMR results, in part, from solution conditions. We emphasize that the observed alterations in the structure of the central helix upon calcium activation are consistent with earlier results that demonstrated an altered proteolytic susceptibility of sites within the central helix upon calcium activation (*80*). The observation that calcium binding causes a decrease in the spatial separation between Trp^{99} and AEDANS bound to Cys^{69} at physiologically relevant ionic strengths is furthermore consistent with previous measurements that have identified a decrease in the Stokes radius and an increase in α-helical content upon calcium activation, which are both modulated by the electrostatic potential of the central helix (*81*, *82*). Furthermore, at acidic pH one observes very similar decreases in the Stokes radius and spatial separation between chromophores positioned near the

Table 3: Rotational Dynamics of AEDANS Bound to Cys^{69} [a]

exptl conditions[b]	ligand	P[c]	r_0	g_1r_0 (ns)	ϕ_1 (ns)	g_2r_0 (ns)	ϕ_2 (ns)	χ^2_R[d]
pH 7.5 + 0.1 M KCl	+calcium	0.073	0.190	0.114	1.9	0.076	12	0.6
		(0.001)	(0.002)	(0.003)	(0.2)	(0.003)	(1)	
	+EGTA	0.078	0.196	0.109	1.9	0.087	13	0.5
		(0.001)	(0.002)	(0.002)	(0.3)	(0.002)	(1)	
pH 7.5 (no KCl)	+calcium	0.073	0.190	0.111	2.0	0.079	13	0.8
		(0.001)	(0.004)	(0.005)	(0.3)	(0.001)	(2)	
	+ EGTA	0.075	0.193	0.121	2.1	0.072	15	0.8
		(0.001)	(0.003)	(0.004)	(0.3)	(0.001)	(3)	
pH 6.3 + 0.1 M KCl	+calcium	0.082	0.187	0.110	1.9	0.077	12	0.5
		(0.001)	(0.004)	(0.004)	(0.2)	(0.003)	(1)	
	+EGTA	0.082	0.191	0.115	1.3	0.076	13	0.5
		(0.001)	(0.003)	(0.003)	(0.4)	(0.003)	(1)	
pH 5.0 + 0.1 M KCl	+calcium	0.077	0.188	0.093	2.1	0.095	14	0.8
		(0.001)	(0.004)	(0.004)	(0.4)	(0.004)	(2)	
	+EGTA	0.078	0.192	0.107	2.1	0.085	15	1.1
		(0.001)	(0.004)	(0.004)	(0.3)	(0.003)	(2)	

[a] Indicated values and associated standard errors of the mean (in parentheses) for three independent measurements were obtained from a two-exponential fit to frequency-domain data collected for AEDANS bound to Cys^{69}, as described in Experimental Procedures (see eq 18). [b] Experimental conditions are as described in Table 1. [c] Steady-state polarization (P). [d] χ^2_R is the average value of the reduced chi squared for a two-exponential fit to the data.

Table 4: Solvent Accessibility of Trp^{99} and AEDANS Bound to Cys^{69} [a]

exptl conditions	ligand	$\langle\tau\rangle$ [b] (ns)	K_{sv} [c] (M^{-1})	$k_q \times 10^{-9}$ [d] (M^{-1} s^{-1})	k_q/k_q (free) [e]
(A) Trp^{99}					
pH 7.5 + 0.1 M KCl	+calcium	4.8 ± 0.1	11.6 ± 0.1	2.42 ± 0.05	0.41 ± 0.01
	+EGTA	5.0 ± 0.1	17.6 ± 0.3	3.52 ± 0.09	0.60 ± 0.02
pH 7.5 (no KCl)	+calcium	4.4 ± 0.1	10.0 ± 0.1	2.29 ± 0.09	0.38 ± 0.01
	+EGTA	4.3 ± 0.1	10.5 ± 0.1	2.42 ± 0.07	0.41 ± 0.01
pH 6.3 + 0.1 M KCl	+calcium	4.5 ± 0.1	9.6 ± 0.1	2.14 ± 0.04	0.36 ± 0.01
	+EGTA	4.9 ± 0.1	11.0 ± 0.1	2.25 ± 0.04	0.38 ± 0.01
pH 5.0 + 0.1 M KCl	+calcium	4.0 ± 0.1	8.6 ± 0.1	2.15 ± 0.06	0.36 ± 0.01
	+EGTA	4.1 ± 0.1	9.8 ± 0.1	2.38 ± 0.07	0.40 ± 0.01
B. AEDANS at Cys^{69}					
pH 7.5 + 0.1 M KCl	+calcium	14.2 ± 0.2	7.0 ± 0.1	0.49 ± 0.03	0.58 ± 0.04
	+EGTA	13.6 ± 0.1	7.2 ± 0.1	0.53 ± 0.03	0.62 ± 0.04
pH 7.5 (no KCl)	+calcium	14.1 ± 0.1	6.8 ± 0.1	0.48 ± 0.01	0.56 ± 0.01
	+EGTA	13.2 ± 0.1	7.1 ± 0.1	0.54 ± 0.01	0.64 ± 0.01
pH 6.3 + 0.1 M KCl	+calcium	13.7 ± 0.1	6.5 ± 0.1	0.47 ± 0.01	0.55 ± 0.01
	+EGTA	13.2 ± 0.1	7.0 ± 0.1	0.53 ± 0.01	0.62 ± 0.01
pH 5.0 + 0.1 M KCl	+calcium	13.7 ± 0.1	5.4 ± 0.1	0.40 ± 0.01	0.47 ± 0.01
	+EGTA	13.2 ± 0.1	5.9 ± 0.1	0.45 ± 0.01	0.53 ± 0.01

[a] Experimental conditions are as described in the legend to Table 1. [b] $\langle\tau\rangle \equiv \sum\alpha_i\tau_i^2/\sum\alpha_i\tau_i$. [c] Quenching data were fit to the following equation $F_0/F = 1 + K_{sv}[Q]$, where F_0 is the initial fluorescence intensity in the absence of acylamide, F is the observed fluorescence intensity at a particular concentration of acylamide, [Q] is the molar concentration of acylamide, and K_{sv} is the Stern−Volmer quenching constant. [d] Bimolecular quenching constants, where $k_q = K_{sv}/\langle\tau\rangle$. [e] Solvent accessibility normalized to the chromophore in solution, where $k_q(\text{NATA}) = 5.9 \times 10^9$ M^{-1} s^{-1} (*91*) and $k_q(\text{AEDANS}) = 8.5 \times 10^8$ M^{-1} s^{-1} (*92*).

Table 5: Rotational Dynamics of Trp^{99} [a]

exptl conditions [b]	ligand	P [c]	r_0	g_1r_0 (ns)	ϕ_1 (ns)	g_2r_0 (ns)	ϕ_2 [d] (ns)	χ^2_R [e]
pH 7.5 + 0.1 M KCl	+calcium	0.24	0.28	0.06	1.1	0.22	⟨12⟩	1.2
		(0.01)	(0.02)	(0.02)	(0.3)	(0.02)		
	+EGTA	0.21	0.28	0.08	1.2	0.20	⟨13⟩	0.8
		(0.01)	(0.01)	(0.02)	(0.2)	(0.01)		
pH 7.5 (no KCl)	+calcium	0.19	0.27	0.03	0.6	0.24	⟨14⟩	3.7
		(0.01)	(0.01)	(0.01)	(0.2)	(0.01)		
	+EGTA	0.17	0.24	0.06	1.3	0.18	⟨15⟩	0.8
		(0.01)	(0.03)	(0.02)	(0.3)	(0.01)		
pH 6.3 + 0.1 M KCl	+calcium	0.23	0.27	0.06	1.6	0.21	⟨12⟩	1.0
		(0.01)	(0.02)	(0.01)	(0.4)	(0.02)		
	+EGTA	0.20	0.28	0.08	1.4	0.20	⟨13⟩	1.1
		(0.01)	(0.01)	(0.02)	(0.2)	(0.02)		
pH 5.0 + 0.1 M KCl	+calcium	0.24	0.29	0.09	0.7	0.20	⟨14⟩	1.4
		(0.01)	(0.02)	(0.01)	(0.2)	(0.01)		
	+EGTA	0.23	0.31	0.08	1.1	0.23	⟨15⟩	0.8
		(0.01)	(0.02)	(0.02)	(0.4)	(0.03)		

[a] Indicated values and associated standard errors of the mean (in parentheses) for three to five independent measurements were obtained from a two-exponential fit to frequency-domain data collected for Trp^{99}, as described in Experimental Procedures (see eq 18). [b] Experimental conditions are as described in Table 1. [c] Steady-state polarization (P). [d] Values of ϕ_2 were independently determined from AEDANS-labeled CaM (see Table 3) and were held fixed in the analysis of the rotational dynamics of Trp^{99}. [e] χ^2_R is the average value of the reduced chi squared for a two-exponential fit to the data. Data were collected at 20 frequencies between 5 and 250 MHz using frequency-independent errors of 0.2° and 0.005 for the differential phase and modulated anisotropy.

ends of the central helix (*83*; Table 1), suggesting the presence of ionizable acidic moieties within the central helix that function to alter the average conformation of CaM. Consistent with this interpretation, we observe a dramatic increase in the conformational heterogeneity within the central helix for apo-CaM at low ionic strength (Figure 5). The observed alterations in CaM structure upon changing the ionic strength are furthermore consistent with previous observations that the addition of monovalent cations alters CaM structure (*27, 73, 74*). Under these latter conditions the role of calcium binding in stabilizing the structure of the central helix is amplified, resulting in a dramatic decrease in conformational heterogeneity (Figure 5D). The observation that calcium binding decreases the spatial separation between chromophores located at opposite ends of the central helix at physiologically relevant ionic strengths is in contrast to previous results, which have suggested that calcium binding results in an elongation of CaM (*6, 84*). This apparent discrepancy may, in part, be related to the calcium-dependent expansion and increased rigidity of the globular domains upon calcium activation (*12, 85*−*87*), which may compensate for the decrease in the dimensions of the central helix following calcium activation. Thus, the decrease in the conformational heterogeneity between opposing globular domains previously reported in wheat germ CaM is consistent with the decreased flexibility of each globular domain following calcium activation (*6*).

The reasons underlying the sensitivity of the structure of the central helix to changes in ionic strength or pH can be understood upon consideration of the structure observed using X-ray crystallography (Figure 8). Consistent with the large amount of conformational disorder observed for apo-

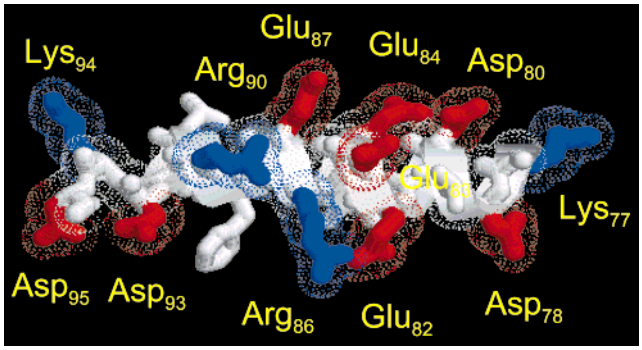

FIGURE 8: Representation of charged residues within the central helix. Acidic (red) and basic (blue) residues within the central helix are depicted within the structure of calcium-saturated CaM (*11*). This illustration was prepared using the coordinates 1cll.pdb and the program RASMOL (*95*).

CaM under conditions of low ionic strength (Figure 5; Table 1), the proximity of the many acidic amino acid side chains (i.e., Asp^{80}, Glu^{82}, Glu^{83}, Glu^{84}, Glu^{87}, Asp^{93}, and Asp^{95}) within the central helix has the potential to destabilize the formation of α-helical secondary structural elements because of the proximal negatively charged carboxylic acid groups. Thus, when the ionic strength is increased, repulsive interactions between these negatively charged carboxylates may be minimized, resulting in a highly ordered α-helical structure stabilized by a range of specific electrostatic interactions that includes short-range hydrogen bonds between α-helical backbone elements. Consistent with this interpretation, scanning calorimetry results have demonstrated that when ^{82}EEE^{84} is replaced by ^{82}KKK,^{84} that there is a decrease in α-helicity that alters the conformational flexibility of CaM (*82*). This result is consistent with previous suggestions that the long-range hydrogen bond between Tyr^{138} and Glu^{82} may play an important role in stabilizing the central helix (*10*, *88*, *89*). Consistent with this latter suggestion, the destabilization of the carboxyl terminus or site-directed replacement of $Tyr^{138} \rightarrow Phe^{138}$ results in a dramatic increase in the conformational heterogeneity in both apo-CaM and calcium-saturated CaM (*89*, *90*). Thus, under normal physiological conditions the association between the high-affinity carboxyl-terminal domain of CaM and target proteins may abolish the long-range hydrogen bond between Tyr^{138} and Glu^{82} (*41*−*43*), thereby disrupting the central helix and facilitating the rapid association of the amino-terminal domain with the proximal binding site on the target protein.

Conclusions and Future Directions. Structurally distinct conformations of the central helix are present in both apo-CaM and calcium-activated CaM at physiological ionic strengths. However, the structure of the central helix is sensitive to changes in ionic strength or pH, indicating the presence of important ionizable groups that may play a role in modulating the stability of the central helix and which may act to facilitate the sequential and ordered binding of the two domains of CaM to target proteins. Future studies should aim to (i) define detailed structural changes within the central helix associated with calcium activation and (ii) identify stabilizing interactions within CaM that may function as molecular triggers to cause the collapse of CaM around target proteins.

REFERENCES

1. James, P., Vorherr, T., and Carafoli, E. (1995) *Trends Biochem. Sci. 20*, 38−42.
2. Finn, B. E., Evenas, J., Drakenberg, T., Waltho, J. P., Thulin, E., and Forsen, S. (1995) *Nat. Struct. Biol. 2*, 777−783.
3. Kuboniwa, H., Tjandra, N., Grzesiek, S., Ren, H., Klee, C. B., and Bax, A. (1995) *Nat. Struct. Biol. 2*, 768−776.
4. Urbauer, J. L., Short, J. H., Dow, K. W., and Wand, A. J. (1995) *Biochemistry 34*, 8099−8109.
5. Zhang, M., Tanaka, T., and Ikura, M. (1995) *Nat. Struct. Biol. 2*, 758−767.
6. Yao, Y., Schöneich, Ch., and Squier, T. C. (1994) *Biochemistry 33*, 7797−7810.
7. Crivici, A., and Ikura, M. (1995) *Annu. Rev. Biophys. Biomol. Struct. 24*, 85−116.
8. Sorensen, B. R., and Shea, M. A. (1996) *Biophys. J. 71*, 3407−3420.
9. Babu, Y. S., Sack, J. S., Greenhough, T. J., Bugg, C. E., Means, A. R., and Cook, W. J. (1985) *Nature 315*, 37−40.
10. Babu, Y. S., Bugg, C. E., and Cook, W. J. (1988) *J. Mol. Biol. 204*, 191−204.
11. Chattopadhyaya, R., Meador, W. E., Means, A. R., and Quiocho, F. A. (1992) *J. Mol. Biol. 228*, 1177−1192.
12. Ikura, M., Spera, S., Barbato, G., Kay, L. E., Krinks, M., and Bax, A. (1991) *Biochemistry 30*, 9216−9228.
13. Barbato, G., Ikura, M., Kay, L. E., Pastor, R. W., and Bax, A. (1992) *Biochemistry 31*, 5269−5278.
14. Klee, C. B. (1977) *Biochemistry 16*, 1017−1024.
15. Seamon, K. B. (1980) *Biochemistry 19*, 207−215.
16. Johnson, J. D. (1983) *Biochem. Biophys. Res. Commun. 112*, 787−793.
17. Yoshida, M., Minowa, O., and Yagi, K. (1983) *J. Biochem. (Tokyo) 94*, 1925−1933.
18. Thulin, E., Andersson, A., Drakenberg, T., Forsen, S., and Vogel, H. J. (1984) *Biochemistry 23*, 1862−1870.
19. Seaton, B. A., Head, J. F., Engelman, D. M., and Richards, F. M. (1985) *Biochemistry 24*, 6740−6743.
20. Heidorn, D. B., and Trewhella, J. (1988) *Biochemistry 27*, 5064−5070.
21. Small, E. W., and Anderson, S. R. (1988) *Biochemistry 27*, 419−428.
22. Wang, C.-L. A. (1989) *Biochemistry 28*, 4816−4820.
23. Yoshino, H., Minari, O., Matsushima, N., Ueki, T., Miyake, Y., Matsuo, T., and Izumi, Y. (1989) *J. Biol. Chem. 264*, 19706−19709.
24. Kataoka, M., Head, J. F., Persechini, A. Kretsinger, R. H., and Engelman, D. M. (1991) *Biochemistry 30*, 1188−1192.
25. MacKall, J., and Klee, C. B. (1991) *Biochemistry 30*, 7242−7247.
26. Maune, J. F., Beckingham, K., Martin, S. R., and Bayley, P. M. (1992) *Biochemistry 31*, 7779−7786.
27. Török, K., Lane, A. N., Martin, S. R., Janot, J.-M., and Bayley, P. M. (1992) *Biochemistry 31*, 3452−3462.
28. Starovasnik, M. A., Su, D. R., Beckingham, K., and Klevit, R. E. (1992) *Protein Sci. 1*, 245−253.
29. Kilhoffer, M., Kubina, M., Travers, F., and Haiech, J. (1992) *Biochemistry 31*, 8098−8106.
30. Pedigo, S., and Shea, M. A. (1995) *Biochemistry 34*, 1179−1196.
31. Pedigo, S., and Shea, M. A. (1995) *Biochemistry 34*, 10676−10689.
32. Shea, M. A., Verhoeven, A. S., and Pedigo, S. (1996) *Biochemistry 35*, 2943−2957.
33. Protasevich, I., Ranjbar, B., Lobachov, V., Makarov, A., Gilli, R., Briand, C., Lafitte, D., and Haiech, J. (1997) *Biochemistry 36*, 2017−2024.
34. Bajzer, Z., and Prendergast, F. G. (1992) *Biophys. J. 65*, 2313−2323.
35. Hennessey, J. P., Manavalan, P., Johnson, W. C., Malencik, D. A., Anderson, S. R., Schimerlik, M. I., and Shalitin, Y. (1987) *Biopolymers 26*, 561−571.
36. Bayley, P. M., and Martin, S. R. (1992) *Biochim. Biophys. Acta 1160*, 16−21.
37. Kretsinger, R. H. (1992) *Cell Calcium 13*, 363−376.

38. Kretsinger, R. H. (1992) *Science 258*, 50−51.
39. Persechini, A., Gansz, K. J., and Paresi, R. J. (1996) *J. Biol. Chem. 271*, 19279−19282.
40. Persechini, A., McMillan, K., and Leakey, P. (1994) *J. Biol. Chem. 269*, 16148−16154.
41. Ikura, M., Clore, G. M., Gronenborn, A. M., Zhu, G., Klee, C. B., and Bax, A. (1992) *Science 256*, 632−638.
42. Meador, W. E., Means, A. R., and Quiocho, F. A. (1992) *Science 257*, 1251−1254.
43. Meador, W. E., Means, A. R., and Quiocho, F. A. (1993) *Science 262*, 1718−1721.
44. Niggli, V., Penniston, J. T., and Carafoli, E. (1979) *J. Biol. Chem. 254*, 9955−9958.
45. Studier, F. W., and Moffatt, B. A. (1986) *J. Mol. Biol. 189*, 113−130.
46. Strasburg, G. M., Hogan, M., Birmachu, W., Thomas, D. D., and Louis, C. F. (1988) *J. Biol. Chem. 263*, 542−548.
47. Hühmer, A. F. R., Gerber, N. C., Ortiz de Montellano, P. R., and Schöneich, Ch. (1996) *Chem. Res. Toxicol. 9*, 484−491.
48. Gornal, A. G., Bardawill, C., and David, M. (1949) *J. Biol. Chem. 177*, 751−766.
49. Lanzetta, P. A., Alverez, L. J., Reinsch, P. S., and Candia, O. (1979) *Anal. Biochem. 100*, 95−97.
50. Yao, Y., Gao, J., and Squier, T. C. (1996) *Biochemistry 35*, 12015−12028.
51. Persechini, A., McMillan, K., and Leakey, P. (1994) *J. Biol. Chem. 269*, 16148−16154.
52. Chapman, E. R., Alexander, K., Vorherr, T., Carafoli, E., and Storm, D. R. (1992) *Biochemistry 31*, 12819−12825.
53. Bayley, P. M., Findlay, W. A., and Martin, S. R. (1996) *Protein Sci. 5*, 1215−1228.
54. Provencher, S. W., and Glöckner, J. (1981) *Biochemistry 20*, 33−37.
55. Provencher, S. W. (1982) *Comput. Phys. Commun. 27*, 229−242.
56. Venyaminov, S. Y., and Yang, J. T. (1990) in *Circular Dichroism and the Conformational Analysis of Biomolecules* (Fasman, G. D., Ed.) pp 69−107, Plenum Press, New York.
57. Gratton, E., and Limkeman, M. (1983) *Biophys. J. 44*, 315−324.
58. Lakowicz, J. R., and Maliwal, B. P. (1985) *Biophys. Chem. 21*, 61−78.
59. Weber, G. (1981) *J. Phys. Chem. 85*, 943−953.
60. Lakowicz, J. R., and Gryczynski, I. (1991) in *Topics in Fluorescence Spectroscopy* (Lakowicz, J. R., Ed.) Vol. I, pp 293−335, Plenum Press, New York.
61. Bevington, P. R. (1969) *Data reduction and Error Analysis for the Physical Sciences*, McGraw-Hill, New York.
62. Luedkte, R., Owen, C. S., Vanderkooi, J. M., and Karush, F. (1981) *Biochemistry 20*, 2927−2936.
63. Haas, E., Katchalski-Katzir, E., and Steinberg, I. (1978) *Biochemistry 17*, 5064−5070.
64. Lakowicz, J. R., Gryczynski, I., Cheung, H. C., Wang, C., Johnson, M. L., and Joshi, N. (1988) *Biochemistry 27*, 9149−9160.
65. Fairclough, R. H., and Cantor, C. R. (1978) *Methods Enzymol. 48*, 347−379.
66. Chabbert, M., Lukas, T. J., Watterson, D. M., Axelsen, P. H., and Prendergast, F. G. (1991) *Biochemistry 30*, 7615−7630.
67. Beechem, J. M., and Haas, E. (1989) *Biophys. J. 55*, 1225−1236.
68. Cheung, H. C. (1991) in *Topics in Fluorescence Spectroscopy* (Lakowicz, J. R., Ed.) Vol. 2, pp 128−176, Plenum Press, New York.
69. Wu, P., and Brand, L. (1992) *Biochemistry 31*, 7939−7947.
70. Lakowicz, J. R., Gryczynski, I., Laczko, G., Wiczk, W., and Johnson, M. L. (1994) *Protein Sci. 3*, 628−637.
71. Wiczk, W. M., Gryczynski, I., Szmacinski, H., Johnson, M. L., Kruszynski, M., and Zboinska, J. (1988) *Biophys. Chem. 32*, 43−49.
72. Johnson, M. L., and Faunt, L. M. (1992) *Methods Enzymol. 210*, 1−37.
73. Sellers, P., Laynez, J., Thulin, E., and Forsén, S. (1991) *Biophys. Chem. 39*, 199−204.
74. Linse, S., Helmersson, A., and Forsén, S. (1991) *J. Biol. Chem. 266*, 8050−8054.
75. Lakowicz, J. R. (1983) *Principles of Fluorescence Spectroscopy*, Plenum Press, New York.
76. Yao, Y., and Squier, T. C. (1996) *Biochemistry 35*, 6815−6827.
77. Beechem, J. M., Gratton, E., Ameloot, M., Knutson, J. R., and Brand, L. (1991) in *Topics in Fluorescence Spectroscopy* (Lakowicz, J. R., Ed.) pp 241−305, Plenum Press, New York.
78. Trewhella, J., (1992) *Cell Calcium 13*, 377−390.
79. Heidorn, D. B., and Trewhella, J. (1988) *Biochemistry 27*, 909−915.
80. MacKall, J., and Klee, C. B. (1991) *Biochemistry 30*, 7242−7247.
81. Crouch, T. H., and Klee, C. B. (1980) *Biochemistry 19*, 3692−3698.
82. Protasevich, I., Ranjbar, B., Lobachov, V., Makarov, A., Gilli, R., Briand, C., Lafitte, D., and Haiech, J. (1997) *Biochemistry 36*, 2017−2024.
83. Sorensen, B. R., and Shea, M. A. (1996) *Biophys. J. 71*, 3407−3420.
84. Small, E. W., and Anderson, S. R. (1988) *Biochemistry 27*, 419−428.
85. Kuboniwa, H., Tjandra, N., Grzesiek, S., Ren, H., Klee, C. B., and Bax, A. (1995) *Nat. Struct. Biol. 2*, 768−776.
86. Zhang, M., Tanaka, T., and Ikura, M. (1995) *Nat. Struct. Biol. 2*, 758−767.
87. Finn, B. E., Evenäs, J., Drakenberg, T., Waltho, J. P., Thulin, E., and Forsén, S. (1995) *Nat. Struct. Biol. 2*, 777−783.
88. Mukherjea, P., Maune, J. F., and Beckingham, K. (1996) *Protein Sci. 5*, 468−477.
89. Gao, J., Yin, D. H., Yao, Y., Sun, H., Qin, Z., Schöneich, Ch., Williams, T. D., and Squier, T. C. (1998) *Biophys. J. 74*, 1115−1134.
90. Sun, H., Yin, D., and Squier, T. C. (1999) *Biophys. J. 76*, A169.
91. Eftink, M. R., and Ghiron, C. A. (1977) *Biochemistry 16*, 5546−5551.
92. Bigelow, D. J., and Inesi, G. (1991) *Biochemistry 30*, 2113-2125.
93. Kraulis, P. J. (1991) *J. Appl. Crystallogr. 24*, 946−950.
94. Fabiato, A. (1988) *Methods Enzymol. 157*, 378−417.
95. Sayle, R. A., and Milner-White, E. J. (1995) *Trends Biochem. Sci. 20*, 374−376.

BI9818671